ISSN 1990-7931, Russian Journal of Physical Chemistry B, 2016, Vol. 10, No. 1, pp. 15–22. © Pleiades Publishing, Ltd., 2016.
Original Russian Text © A.E. Galashev, V.A. Polukhin, 2016, published in Khimicheskaya Fizika, 2016, Vol. 35, No. 2, pp. 18–25.

STRUCTURE OF CHEMICAL
COMPOUNDS. SPECTROSCOPY

Simulation of the Removal of a Lead Film from Graphene by the Irradiation of a Target with a Beam of Xenon Clusters

A. E. Galashev[a, *] **and V. A. Polukhin**[b]
[a] *Institute of High Temperature Electrochemistry, Ural Branch, Russian Academy of Sciences, Yekaterinburg, 620219 Russia*
[b] *Institute of Materials Science and Metallurgy, Yeltsin Ural Federal University, Yekaterinburg, 620002 Russia*
**e-mail: alexander-galashev@yandex.ru*

Received November 24, 2014

Abstract—The removal of a lead film from graphene by irradiating a target with a beam of xenon clusters at an incidence angle of 60° was studied by the molecular dynamics method. The complete purification of graphene was achieved at beam energies of 10 and 15 eV. Visual observation and the calculated density profiles and mobility components of the lead atoms indicate the predominantly collective nature of the separation of Pb from graphene in the course of bombardment. When a beam of clusters with an energy of 15 eV acts on the target, the detached film of lead takes a torch shape and has strong internal stresses. The graphene sheet acquires maximum roughness at a beam energy of 10 eV as a result of a large number of the direct hits of xenon clusters on its surface.

Keywords: graphene, xenon cluster, stress, film, lead
DOI: 10.1134/S1990793116010164

INTRODUCTION

The trace amounts of metals always occur in the natural biosphere. The presence of some of them even in a low concentration requires rapid oxidation because metals in higher concentrations and products in low oxidation states can be toxic and dangerous. Unfortunately, difference between permissible and dangerous concentration levels is small [1, 2]. PbS belongs to the most frequently occurring trace compounds in nature. It is used in electrical batteries, small arms, and X-ray units and as a pigment in domestic metallic mixtures. The detection of industrial lead in the environment is of considerable importance. Until now, lead has been determined by various methods such as spectrophotometry [3, 4], liquid–liquid extraction [5, 6], turbidimetry [7, 8], and electrochemical measurements [9]. Some of these methods are inaccurate because of the low limits of detection and harmful solvents. In recent years, solid-phase extraction has been used for the determination of Pb traces. The trace amounts of Pb in aqueous media are detected with the aid of a surfactant covered with modified f-OH graphene.

The negligibly small amounts of heavy metals can be removed from air and water using filters with graphene membranes. However, in this case, the filters should be subsequently cleaned for the removal of a metal deposit. Lead has a low energy of adhesion with perfect graphene (0.2 eV) [10]; however, the binding energy of Pb atoms with graphene at a divacancy boundary is very considerable (3.4 eV) [11]. A heavy metal film can be removed from graphene by the bombardment of the latter with noble gas clusters [12–15]. The simulation of a cluster bombardment process showed that the energy transferred upon the impact should be entirely released in a critical region near the surface in order to obtain a maximum effect [16–18]. It was experimentally demonstrated that, on the incidence of a beam of Xe atoms onto the surface of graphite at an incidence angle of 55°, the energy transferred to the phonon modes of the surface is approximately 20% smaller than that in the case of a vertically directed beam [19]. In this case, the Xe atoms are scattered on the smooth surface of graphite even at energies of several tens of eV. In order to decrease the probability of damaging graphene upon the bombardment of a lead–graphene film, we selected an incidence angle of 60°. The energies of the cluster beams used were much lower than the energies of beams in the experiments oriented to the sputtering of a bombarded substance.

The aim of this work was to study in detail the process of the removal of a lead film from partially hydrogenated imperfect graphene without destroying this latter.

MOLECULAR DYNAMICS MODEL

The interatomic interactions in graphene were represented by the modified Tersoff many-body potential [20]. This potential is based on the concept of binding order. The potential energy between the two neighboring atoms *i* and *j* is written as

$$V_{ij} = f_C(r_{ij})\left[A\exp(-\lambda^{(1)}r_{ij}) - Bb_{ij}\exp(-\lambda^{(2)}r_{ij})\right],$$

$$f_C(r_{ij}) = \begin{cases} 1, & r_{ij} < R^{(1)} \\ \dfrac{1}{2} + \dfrac{1}{2}\cos\left[\pi\left(r_{ij} - R^{(1)}\right)\big/(R^{(2)} - R^{(1)})\right], & R^{(1)} < r_{ij} < R^{(2)}, \\ 0, & r_{ij} > R^{(2)}, \end{cases} \qquad (1)$$

$$b_{ij} = (1 + \beta^n \xi_{ij}^{n_i})^{-1/(2n)}, \quad \xi_{ij} = \sum_{k\neq i,j} f_C(r_{ij})g(\theta_{ijk}), \quad g(\theta_{ijk}) = 1 + \frac{c^2}{d^2} - \frac{c^2}{\left[d^2 + (h - \cos\theta_{ijk})^2\right]}.$$

Here, the subscripts $i, j,$ and k refer to carbon atoms; r_{ij} is the i–j bond length; and θ_{ijk} is the angle between the i–j and j–k bonds. The parameters of Eq. (1) other than the quantity $R^{(2)}$ were taken from Ref. [21].

A change to the simulation of two-dimensional systems (for example, to the simulation of graphene) with covalent bonds requires the modification of this potential [22]. In the present model, the maximum scope ($R^{(2)}$) of covalent interaction was increased from 0.21 to 0.23 nm. Beyond the scope of covalent interaction, very weak Lennard-Jones attractive interaction with the parameters taken from Ref. [21] had an effect. For averting the rotation of a graphene sheet, retardation with the force $-dV_{ij}(\Omega_{kijl})\big/dr_{ij}$, where the torsional potential $V_{ij}(\Omega_{kijl})$ was determined by Stuart et al. [21], at each atomic site of graphene was used.

For the simulation of atomic interactions in the film of lead, we used the Sutten–Chen many-body potential [23]. The Sutten–Chen potential energy is written as

$$U^{SC} = \varepsilon\left[\frac{1}{2}\sum_i\sum_{j\neq i}V(r_{ij}) - c\sum_i\sqrt{\rho_i}\right],$$

where

$$V(r_{ij}) = (a/r_{ij})^q, \quad \rho_i = \sum_{j\neq i}(a/r_{ij})^s;$$

ε is a parameter with the dimensionality of energy; c is a dimensionless parameter; a is a parameter with the dimensionality of length, which is usually chosen equal to the lattice constant; and q and s are positive integers, $q > s$. The exponential form of contributions makes it possible to successfully combine short-range interactions, which are represented by an N-particle term, with the van der Waals "tail," which is responsible for long-range interaction.

The lead–carbon and xenon–xenon interactions were given by the Lennard-Jones potential [24–26]. The interaction between Xe atoms and target atoms (Pb and C) was determined by the purely repulsive ZBL potential (see [27])

$$\begin{aligned}\Phi = Z_iZ_j\frac{e^2}{r}\Big\{&0.1818\exp\left(-3.2\frac{r}{a}\right) \\ &+ 0.5099\exp\left(-0.9423\frac{r}{a}\right) \\ &+ 0.2802\exp\left(-0.4029\frac{r}{a}\right) \\ &+ 0.02817\exp\left(-0.2016\frac{r}{a}\right)\Big\},\end{aligned}$$

where Z_i and Z_j are the atomic numbers of the ith and jth atoms, respectively; e is the elementary electric charge; r is the interatomic distance; and the parameter a is determined by the expression

$$a = 0.8854a_0\left(Z_i^{0.23} + Z_j^{0.23}\right)^{-1}.$$

Here, a_0 is the Bohr radius. We disregard weak attraction between the Xe and Pb atoms and also between the Xe and C atoms because the primary aim of this study is to study the transfer of energy and angular momentum rather than chemical binding [28].

Defects substantially enhance the adhesion of metals to graphene. The most frequent defects in graphene are divacancies. The sheet of graphene used for the deposition of lead had four divacancies rather uniformly distributed over its surface. Hydrogenation was used for the strengthening of divacancy edges and boundaries. The CH groups formed at the edges and sites nearest to the divacancy center were simulated in accordance with the monatomic diagram [29]. The C–CH and CH–CH interactions were represented by the Lennard-Jones potential [29]. The partial functionalization of graphene in the form of the addition of hydrogen atoms to its edges stabilizes the structure without leading to an increase in interatomic distances and without creating roughness over the entire surface.

The formation of a film of lead on graphene in a single molecular dynamics (MD) calculation occurred into two stages. At the first stage, Pb atoms were placed above the centers of nonadjacent graphene cells so that the distance between Pb and C atoms was equal to a of distance 2.33 Å calculated according to the density functional theory [11]. Additional 51 atoms of Pb were randomly deposited onto this friable film of lead that consisted of 49 atoms of Pb. Then, the system of 100 atoms of Pb and 406 atoms of C was equilibrated in an MD calculation with a duration of 1 million time steps ($\Delta t = 0.2$ fs). The numerical solution of the equations of motion was carried out by the fourth-order Runge–Kutta method. The target thus obtained was subsequently bombarded with Xe_{13} icosahedral clusters. As a result of two-dimensional uniform extension, the flat sheet of graphene is torn up with the formation of zigzag and armchair edges, which are determined by the structure of the atomic lattice of the material. We selected the directions parallel to these edges as the x and y axes, respectively. Five starting points for positioning the centers of Xe_{13} clusters were evenly spread on a line parallel to the y axis (the armchair direction). This line was shifted to the left (along the x axis) from the left edge of graphene at a distance of 1.5 nm and raised to a height (in the direction of the z axis) in order to reach the angle $\varphi = 30°$ between the x axis, which passes near the upper film surface, and the impact direction line. The interval equal to the length of the graphene sheet in the direction of the x axis (the zigzag direction) was divided into five equal sections with the length $L_i = L_x/5$. At the beginning of each following cycle of cluster impacts, the line of the starting points of Xe_{13} clusters moved horizontally forward to the distance L_i. As a result, the film surface approximated by a plane was covered with 25 evenly distributed points, to which cluster impacts were aimed. Each series included 5 cycles or 25 impacts. At the starting points, all of the atoms of an Xe_{13} cluster acquired the same velocity, which determined the direction of impact. The clusters were directed toward the target in turn. The lifetime (determined as the sum of the transit time and the time of interaction with the target) of each cluster was 8 ps. After this time, the Xe atoms of a destroyed cluster were excluded from consideration, and the new Xe_{13} cluster began motion from another starting point. A cycle of five cluster bombardments required 40 ps, whereas a series (of five cycles) required 0.2 ns (we will subsequently designate the impact number in the series as n), ant the entire bombardment (of five series) took 1 ns. Bombardment at five different cluster energy values of 5, 10, 15, 20, and 30 eV was performed at the incidence angle $\theta = 60°$.

The impacts of clusters with the surface were accompanied by the heating of the system. The moderate removal of the released heat from the system was performed in accordance with the Berendsen model with the binding constant $\tau = 4$ fs [30]. In order to control heating, the velocities v at each time step were scaled according to the expression

$$v' = \lambda v, \quad \lambda = \left[1 + \frac{\Delta t}{\tau}\left(\frac{T_0}{T} - 1\right)\right]^{1/2},$$

where v' and v are the new and current velocities, respectively; λ is the scaling factor; T_0 is the assigned temperature (300 K); and T is the current temperature.

The density profile of metallic film was determined as

$$\rho(z) = \frac{n(z)\sigma_{Pb}^3}{\Delta h S_{xy} N_s},$$

where $n(z)$ is the number of Pb atoms in a layer parallel to the graphene plane; σ_{Pb} is the effective atomic diameter of Pb; Δh is the width of the layer; S_{xy} is the surface area of graphene; and N_s is the number of tests.

The partial coefficient of atomic diffusion is calculated as [31]

$$D = D_{xy} + D_z = \frac{1}{2\Gamma\tau}\left\langle [\Delta \mathbf{r}(t)]^2 \right\rangle_p,$$

where $\Gamma = 3$ is the dimensionality of space, $\langle \ldots \rangle$ denotes averaging over p, where p is the number of time intervals for the determination of $\left\langle [\Delta \mathbf{r}(t)]^2 \right\rangle$. We performed the averaging of five time dependences, each of which was calculated in the interval $\tau = 200$ ps.

Stress in the position of the ith atom of metallic film is determined as [23]

$$\sigma_{\alpha\beta}(i) = \frac{\varepsilon}{2a^2\Omega_i}\sum_{i \neq j}^{k}\Big[-q\left(a/r_{ij}\right)^{q+2} + cs\left(1/\sqrt{\rho_i} + 1/\sqrt{\rho_j}\right)\left(a/r_{ij}\right)^{s+2}\Big] r_{ij}^{\alpha} r_{ij}^{\beta},$$

where the volume Ω_i of an individual atom can be associated with the volume of the Voronoi polyhedron related to the ith atom.

For the calculation of stresses that appear in graphene, the graphene sheet was divided into the surface elements. The stresses $\sigma_{u\alpha}(l)$, which appear under the action of forces in the direction $\alpha = x, y, z$, were calculated on each surface element with the number l, which has the orientation u. In these calculations, the products of the projections of the velocities of atoms and the projections of the forces f_{ij}^{α}, which act on the element l from other atoms, were used when the following conditions were satisfied [32]:

$$\sigma_{u\alpha}(l) = \left\langle \sum_{i}^{k} \frac{1}{\Omega}\left(m \mathrm{v}_u^i \mathrm{v}_\alpha^i\right) \right\rangle + \frac{1}{S_l}\left\langle \sum_{i}^{k} \sum_{j \neq i}^{(u_i \leq u, u_j \geq u)} \left(f_{ij}^{\alpha}\right) \right\rangle. \tag{2}$$

Here, k is the quantity of atoms in the surface element l; Ω is the volume per atom; m is the mass of an atom, v_α^i is the α projection of the velocity of the ith atom; and S_l is the surface area of the element l. The conditions of summation over j in the latter sum of expression (2) are reflected in both the subscript and the superscript of the sum; the force that appears on the interaction of ith and jth atoms passes through the sur-

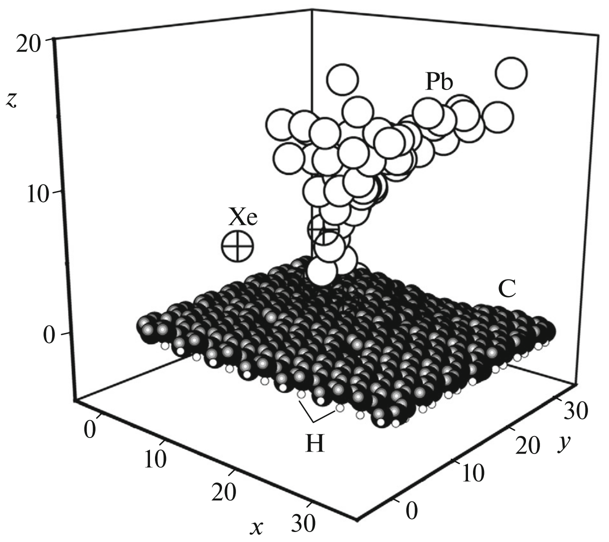

Fig. 1. Configuration of the lead film–partially hydrogenated graphene system after bombardments at an incidence angle of 60° with a 15-eV Xe_{13} cluster energy.

face element l; u_i is the moving coordinate of the ith atom; in the superscript of the sum, u designates the coordinate of the point of contact of the straight line that passes through the centers of the ith and jth atoms with the surface element l. The compressive stresses on this determination can have the sign + or – in accordance with the directions of the forces f_J^i. This is the difference of the microscopic stress $\sigma_{uJ}(l)$, from the macroscopic stress $\bar{\sigma}_J < 0$. The total stresses, which act in the plane of graphene, were determined by the summing up of the corresponding elementary stresses:

$$\sigma_{zJ} = \sum_{l=1}^{N_l} \sigma_J^z(l),$$

where N_l is the number of surface elements on the discretization of the sheet of graphene in a selected direction.

The surface roughness (or the arithmetic mean of a profile deviation) was calculated as

$$R_a = \frac{1}{N}\sum_{i=1}^{N} |z_i - \bar{z}|,$$

where N is the number of sites (atoms) on the surface of graphene, z_i is the displacement of the ith atom in the direction of the z axis; and $\bar{z}$ is the average value of the coordinate z for grapheme; the values of z_i and $\bar{z}$ were determined at the same point in time.

The total energy of free one-sheet graphene obtained at $T = 300$ K was –7.02 eV, which is consistent with the result of a quantum-mechanical calculation (–6.98 eV) [33]. The melting temperature (T_m) of a Pb_{201} cluster with a free surface, which was determined in a special calculation, was 417 K, which is consistent with MD calculations ($T_m = 412$ K) [34], which were also performed with the Sutten–Chen potential. In both cases, T_m was determined based on a potential energy jump.

RESULTS OF THE CALCULATION

As a result of bombardment with 5-eV Xe_{13} clusters, the film of Pb remained on the graphene. In this case, a small part of metal atoms was knocked out from the film, and the film itself was bent to keep contact with graphene only in its middle part; that is, the film edges became raised.

Bombardment with a beam energy of 10 eV led to the complete separation of a Pb film from graphene. Only an insignificant part of the Pb atoms was knocked out from the film, and the major portion went away in the form of a dense cluster.

In general, a similar behavior was also observed on the bombardment with a beam energy of 15 eV (Fig. 1). However, in this case, the major portion of the film was immediately detached away from graphene to a small distance. Because it was conically shaped expanded upwards, it was again forced against graphene at the cone apex under the impacts of Xe_{13} clusters.

We found that a further increase in the cluster beam energy did not facilitate the removal of a Pb film from graphene. Thus, as a result of bombardment with an energy of 20 eV, the film was not separated from graphene with a loss of a portion of individual knocked-on atoms. Two atoms were stuck in divacancies, and they helped to retain the film on graphene by attracting the other Pb atoms. The film had close contact with graphene at the center. The film edges were elevated.

The released 30-eV Xe_{13} clusters crushed the film of lead and pushed several Pb atoms through divacancies. A small lead cluster was arranged at the front edge of graphene without loss in binding with the base layer. Because of hydrogenation, the graphene edges remained intact even after bombardment with an energy of 30 eV.

Figure 2 demonstrates the vertical profiles of density. Bombardment with a cluster energy of 5 eV left a sufficiently monolithic film on graphene. Moreover, in the course of bombardment, the Pb atoms located in the lattice dimples of the honeycomb type formed by C atoms, retained their positions, as evidenced by a sharp peak at 0.237 nm. A small number of single atoms descended into divacancies or moved away from the film, as confirmed by the presence of separate low peaks.

Approximately the same pattern of the arrangement of Pb atoms was observed at a 10-eV energy of

Xe_{13} clusters. The film thickness increased due to swelling under the impacts of the clusters, and the number of separated Pb atoms increased. At the end of the bombardment, the film separated from graphene and rapidly moved away to a distance greater than 1 nm. The new film position is not reflected in the profile $\rho(z)$.

The rapid rise of the entire film at the distance $r >$ 0.3 nm over graphene occurred at the energy of bombarding clusters of 15 eV. The density profile as a whole was shifted to the right.

At the cluster beam energies $E_{Xe} > 15$ eV, the film was either unseparated from graphene (20 eV) or broken into separate pieces (30 eV). At an energy of 20 eV, a noticeable number of the Pb atoms were pushed through divacancies, and single scattered Pb atoms were also present. The penetration of lead atoms to the reverse side of graphene was insignificant at energies of 30 eV. In this case, the knocked out film pieces rapidly moved away to distances greater than 1 nm, and they are not reflected in the profile $\rho(z)$.

The horizontal component D_{xy} of the mobility of Pb atoms tends to decrease as the energy of bombarding clusters is increased up to 20 eV (Fig. 3). However, the value of D_{xy} sharply increases at a cluster energy of 30 eV. This fact is indicative of a change in the nature of deformation in the film of lead under the action of a cluster beam. The vertical component D_z of the mobility of Pb atoms does not exhibit such a pronounced lift at a beam energy of 30 eV, but it manifests a sharp burst at an energy of 10 eV. This burst is caused by the detachment and rapid removal of the major portion of the film from graphene. In general, the vertical component of the mobility of Pb atoms is lower by almost an order of magnitude than the horizontal mobility.

The curves of $D_{xy}(E_{Xe})$ and $D_z(E_{Xe})$ for the C atoms in graphene (Fig. 4) are mainly consistent in shape with analogous curves for the Pb atoms (Fig. 3). The presence of a local minimum at $E_{Xe} = 15$ eV in place of a local maximum in the curve of $D_{xy}(E_{Xe})$ for graphene is the exception. Furthermore, at low energies ($E_{Xe} \leqslant 10$ eV), the values of D_{xy} are even higher than those at the energy $E_{Xe} = 30$ eV, where the Pb atoms injected into dimples produce local pressing and decrease the mobility of the C atoms in horizontal directions. A burst in the function $D_z(E_{Xe})$ at $E_{Xe} = 10$ eV for graphene is impressive such as that in an analogous function for lead. This is most likely indicative of the fact that the impacts of Xe_{13} clusters, which caused the detachment and rapid withdrawal of the film, arrived directly at the graphene surface, and the Xe_{13} atoms scattered upward and in the opposite direction pushed the loosely lying Pb film and removed it from graphene. An insignificant increase in the value of D_z for the C atoms at the energy $E_{Xe} = 30$ eV is related to

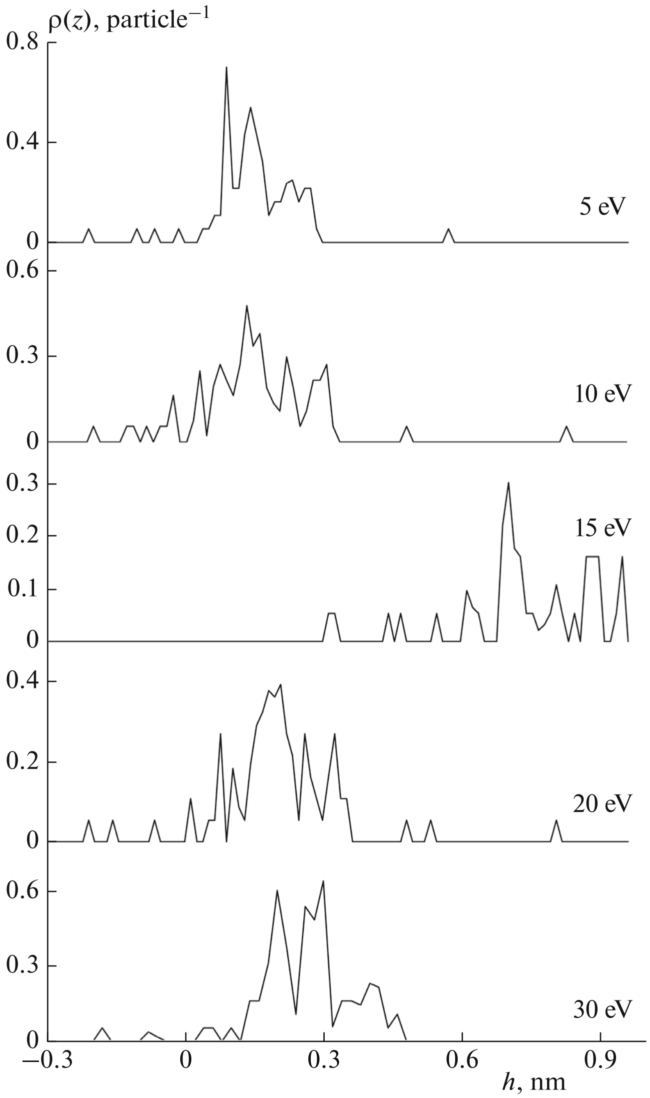

Fig. 2. Lead film density profiles obtained in the course of the cluster bombardments of a target with different energies. The Level $h = 0$ corresponds to the vertical mark of the presence of C atoms in graphene.

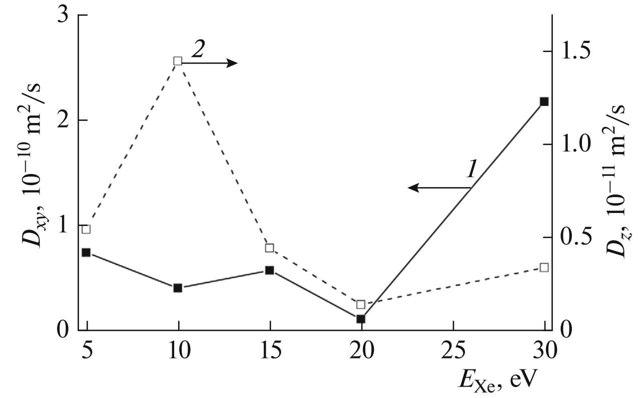

Fig. 3. Horizontal D_{xy}, and vertical D_z components of the coefficient of mobility of Pb atoms obtained as a result of the entire bombardment as functions of the energy of bombarding Xe_{13} clusters.

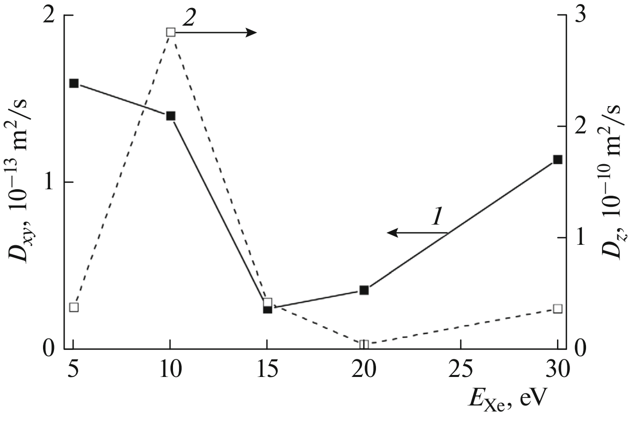

Fig. 4. Horizontal D_{xy}, and vertical D_z components of the coefficient of mobility of the C atoms of graphene as functions of the energy of bombarding Xe_{13} clusters.

the presence of rigid C–C bonds and the absence of graphene integrity damage.

The study of the evolution of the stresses σ_{zx}, σ_{zy}, and σ_{zz} in the cases of the removal of a Pb film from graphene (E_{Xe} = 10 and 15 eV) showed that their smooth relaxation occurred only during the first series of impacts. Already in the course of the third series of impacts, strong changes in the stresses created by horizontal forces (σ_{zx} and σ_{zy}) were observed, especially at the final stage. In this case, the stress created by vertical forces (σ_{zz}) increased much more successively. In the course of the fifth series of bombardment, the stresses σ_{zx} and σ_{zy} became even more significant. Over the course of this series, the stresses σ_{zz} strengthened almost continuously. In general, the stresses σ_{zx}, σ_{zy}, and σ_{zz} in graphene along the *x* axis obtained after the fifth series of impacts were no higher than the stresses resulting from the first series of bombardment. In other words, in the course of the entire bombardment, an increase in the local stresses in graphene was not observed. Note that the value of the stresses σ_{zz} created by vertical forces was much greater (by a factor of to ~2) than the stresses σ_{zx} and σ_{zy}, which appeared due to the application of horizontal forces.

In view of a specific shape taken by the film of lead after bombardment with an energy of 15 eV, the final stresses σ_{zx} and σ_{zz} in the film were considerably different from analogous stresses obtained after bombardments with other energies of the Xe_{13} clusters (Fig. 5). At the same time, the function $\sigma_{zy}(E_{\mathrm{Xe}})$ has a smooth shape; that is, the value of σ_{zy} at E_{Xe} = 15 eV is not strongly different from the values of this stress obtained at other E_{Xe}. All of the three stresses have values of the same order of magnitude (in the majority of cases, the absolute value of σ_{zz} is somewhat greater) with the exception of the value of σ_{zy} at E_{Xe} = 15 eV.

The dependence of the resulting stresses σ_{zx}, σ_{zy}, and σ_{zz} in graphene on the energy E_{Xe} only partially correlates with the behavior of analogous characteristics in a Pb film (Fig. 6). The behavior of only the quantity σ_{zz} is similar in many respects to that of the corresponding stress in the metallic film. Here, a dip of the curve of $\sigma_{zz}(E_{\mathrm{Xe}})$ into the region of negative values was also observed at E_{Xe} = 15 eV. However, the value of σ_{zz} did not reach positive values at E_{Xe} = 20 eV, as was the case in the film of lead. The function $\sigma_{zx}(E_{\mathrm{Xe}})$, was characterized by a smoother behavior, whereas the function $\sigma_{zy}(E_{\mathrm{Xe}})$ for the film of Pb exhibited this

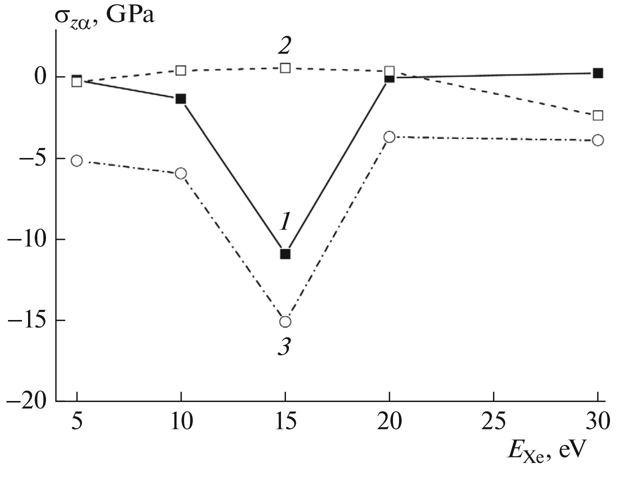

Fig. 5. Basic stresses (*1*) σ_{zx}, (*2*) σ_{zy}, and (*3*) σ_{zz} in the film of Pb obtained as a result of the complete bombardment as functions of the energy of bombarding Xe_{13} clusters.

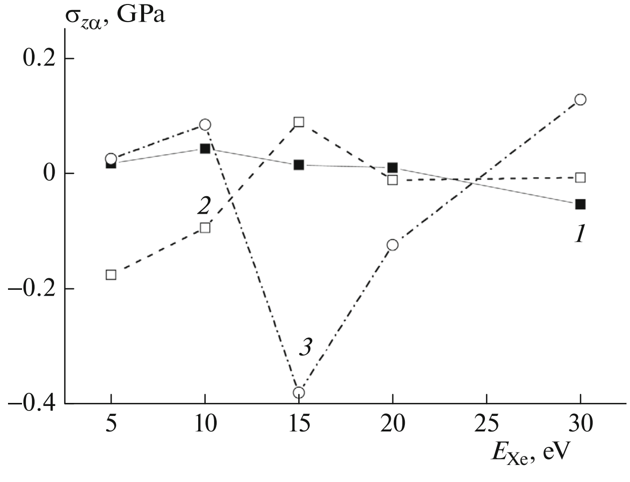

Fig. 6. Basic stresses (*1*) σ_{zx}, (*2*) σ_{zy}, and (*3*) σ_{zz} in graphene obtained as a result of the complete bombardment as functions of the energy of bombarding Xe_{13} clusters.

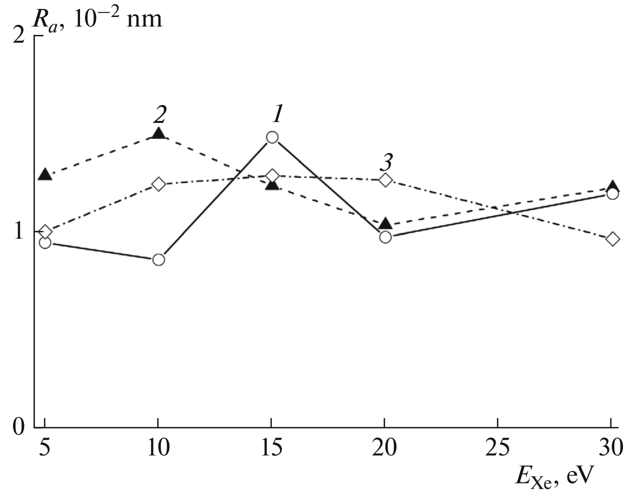

Fig. 7. Dependence of the roughness of graphene on the energy of bombarding Xe_{13} clusters at the incidence angles of (*1*) 0°, (*2*) 60°, and (*3*) 90°.

property. The function $\sigma_{zy}(E_{Xe})$ for graphene exhibited a maximum at $E_{Xe} = 15$ eV. The largest negative stress (σ_{zy}) caused by horizontal forces in the direction of the *y* axis appeared at $E_{Xe} = 5$ eV, and stress of the same sign from vertical forces (σ_{zz}) appeared at $E_{Xe} = 15$ eV.

As a rule, the roughness of graphene R_a increased with the energy E_{Xe} on the bombardment of a target at the angle of incidence $\theta = 60°$ (Fig. 7). The maximum roughness reached at $E_{Xe} = 10$ eV was caused by the early detachment of a Pb film from graphene, as a result of which graphene directly took a great number of the impacts of Xe_{13} clusters. Figure 7 compares the function $R_a(E_{Xe})$ at $\theta = 60°$ with analogous functions obtained at incidence angles of 0° and 90°, i.e., with the vertical and horizontal directions of bombardment. Difference in the roughness of graphene subjected to uniform (in terms of Xe_{13} cluster energy and intensity) bombardment with different angles of incidence can be greater than 40% (at $E_{Xe} = 10$ eV). The smooth function $R_a(E_{Xe})$ was obtained upon low-level bombardment; in this case, a roughness maximum was reached at $E_{Xe} = 15$ eV.

CONCLUSIONS

In this work, we studied five versions of the bombardment of a Pb film on graphene with Xe_{13} clusters with energies from 5 to 30 eV. The best cleaning effect was achieved at $E_{Xe} = 10$ eV. The Pb film can also be removed (on point contact) at a cluster energy of 15 eV. The use of higher beam energies is ineffective because of the pushing of Pb atoms into divacancies and the impression of the metal atoms into dimples on graphene. The hydrogenated edges of graphene do not acquire noticeable damage even after the bombardment with 30-eV Xe_{13} clusters. For example, unlike copper, the prevailing mechanism in the process of lead removal is the detachment of the major portion of a film from graphene rather than the knocking out of separate Pb atoms. This is evident from an analysis of the density profiles of the system and the energy dependence of the mobility components of Pb atoms. The bombardment of graphene after the removal of a film leads to a considerable increase in the vertical component of the mobility of the C atoms. Stresses in the lead film that remained on graphene increased in the course of bombardment, whereas analogous stresses in graphene were not accumulated with time. The highest stresses occurred in the detached film of lead, which increased its vertical size and took a torch shape, as a result of the action of both vertical and horizontal forces. In this case, an increase in the internal stress was also extended to graphene. The graphene subjected to direct bombardment with 10-eV Xe_{13} clusters acquired the greatest roughness as a result of the rapid removal of the Pb film.

ACKNOWLEDGMENTS

This work was supported by the Russian Foundation for Basic Research (project no. 13-08-00273).

REFERENCES

1. S. N. Luoma, Sci. Total Environ. **28**, 1 (1983).
2. W. Hummers and R. Offeman, J. Am. Chem. Soc. **80**, 1339 (1985).
3. Y. S. Choi and H. S. Choi, Bull. Korean. Chem. Soc. **24**, 222 (2003).
4. L. Zaijan, Y. Yuling, T. Jian, and P. Jiaomai, Talanta **60**, 123 (2003).
5. D. Kara, M. Alkan, and U. Cakir, Turk. J. Chem. **25**, 293 (2001).
6. S. B. Sonawale, Y. V. Ghalsasi, and A. P. Argekar, Anal. Sci. **17**, 285 (2001).
7. J. L. Manzoori and A. Bavili-Tabrizi, Microchem. J. **72**, 1 (2002).
8. J. Chen and K. C. Teo, Anal. Chim. Acta **450**, 215 (2001).
9. S. Yuan, W. Chen, and S. Hu, Talanta **64**, 922 (2004).
10. H. Gao, J. Zhou, M. Lu, W. Fa, and Y. Chen, J. Appl. Phys. **107**, 114311 (2010).
11. D. Ma and Z. Yang, New J. Phys. **13**, 123018 (2011).
12. A. E. Galashev and V. A. Polukhin, J. Surf. Invest.: X-ray, Synchrotr. Neutron Tech. **8**, 1078 (2014).
13. A. E. Galashev and V. A. Polukhin, Phys. Met. Metallogr. **115**, 697 (2014).
14. A. E. Galashev and O. R. Rakhmanova, Phys. Usp. **57**, 970 (2014).
15. A. E. Galashev and A. A. Galasheva, High Energy Chem. **48**, 112 (2014).

16. M. F. Russo, Jr. and B. J. Garrison, Anal. Chem. **78**, 7206 (2006).
17. M. F. Russo, Jr., C. Szakal, J. Kozole, N. Winograd, and B. J. Garrison, Anal. Chem. **79**, 4493 (2007).
18. E. J. Smiley, N. Winograd, and B. J. Garrison, Anal. Chem. **79**, 494 (2007).
19. Y. Watanabe, H. Yamaguchi, M. Hashinokuchi, et al., Chem. Phys. Lett. **413**, 331 (2005).
20. J. Tersoff, Phys. Rev. Lett. **61**, 2879 (1988).
21. S. J. Stuart, A. V. Tutein, and J. A. Harrison, J. Chem. Phys. **112**, 6472 (2000).
22. V. A. Polukhin and N. A. Vatolin, Russ. Chem. Rev. **84**, 498 (2015).
23. H. Rafii-Tabar, Phys. Rep. **325**, 239 (2000).
24. Y. M. Kim and S.-C. Kim, J. Korean Phys. Soc. **40**, 293 (2002).
25. A. Arkundato, Z. Su'ud, M. Abdullah, and W. Sutrisno, Int. J. Appl. Phys. Math. **3**, 1 (2013).
26. F.-Y. Li and R. S. Berry, J. Phys. Chem. **99**, 2459 (1995).
27. J. F. Ziegler, J. P. Biersack, and U. Littmark, *Stopping and Ranges of Ions in Matter* (Pergamon, New York, 1985), Vol. 1.
28. A. Delcorte and B. J. Garrison, J. Phys. Chem. B **104**, 6785 (2000).
29. F. D. Lamari and D. Levesque, Carbone **49**, 5196 (2011).
30. H. J. C. Berendsen, J. P. M. Postma, W. F. van Gunsteren, A. DiNola, and J. R. Haak, J. Chem. Phys. **81**, 3684 (1984).
31. A. E. Galashev, Comput. Mater. Sci. **98**, 123 (2015).
32. B. Hafskjold and T. Ikeshoji, Phys. Rev. E **66**, 011203 (2002).
33. S. Yu. Davydov, Phys. Solid State **54**, 875 (2012).
34. Z. H. Jin, H. W. Sheng, and K. Lu, Phys. Rev. B **60**, 141 (1999).

Translated by V. Makhlyarchuk